© 2023. Published by The Company of Biologists Ltd | Development (2023) 150, dev201572. doi:10.1242/dev.201572

RESEARCH ARTICLE

PATL2 regulates mRNA homeostasis in oocytes by interacting with EIF4E and CPEB1

Zhihua Zhang[1,*], Ruyi Liu[1,*], Hongbin Zhou[1,*], Qun Li[1], Ronggui Qu[1], Weijie Wang[1], Zhou Zhou[1], Ran Yu[1], Yang Zeng[1], Jian Mu[1], Biaobang Chen[2], Xuejiang Guo[3,‡], Qing Sang[1,‡] and Lei Wang[1,‡]

ABSTRACT

The accumulation and storage of maternal mRNA is crucial for oocyte maturation and embryonic development. PATL2 is an oocyte-specific RNA-binding protein, and previous studies have confirmed that *PATL2* mutation in humans and knockout mice cause oocyte maturation arrest or embryonic development arrest, respectively. However, the physiological function of PATL2 in the process of oocyte maturation and embryonic development is largely unknown. Here, we report that PATL2 is highly expressed in growing oocytes and couples with EIF4E and CPEB1 to regulate maternal mRNA expression in immature oocytes. The germinal vesicle oocytes from *Patl2*$^{-/-}$ mice exhibit decreasing maternal mRNA expression and reduced levels of protein synthesis. We further confirmed that PATL2 phosphorylation occurs in the oocyte maturation process and identified the S279 phosphorylation site using phosphoproteomics. We found that the S279D mutation decreased the protein level of PATL2 and led to subfertility in *Patl2*^{S279D} knock-in mice. Our work reveals the previously unrecognized role of PATL2 in regulating the maternal transcriptome and shows that phosphorylation of PATL2 leads to the regulation of PATL2 protein levels via ubiquitin-mediated proteasomal degradation in oocytes.

KEY WORDS: PATL2, Oocyte, Maternal mRNA, Phosphorylation, Female infertility, Mouse

INTRODUCTION

The proper accumulation, storage, translation and degradation of maternal mRNA is essential for oocyte maturation and embryonic development (Coticchio et al., 2015; Sha et al., 2020). After birth, oocytes are maintained in prophase I, which is the period of oocyte growth. During this phase, the oocyte grows rapidly in size and mass accompanied by a dramatic increase in transcriptional activity (Picton et al., 1998), and the oocyte accumulates the maternal mRNA required for subsequent maturation and embryonic development. To prevent premature activation of the developmental program, the maternal mRNAs are translationally silenced by shortening the length of the poly(A) tail, which causes them to be transported into the cytoplasm and sequestered into storage in cytoplasmic granules (Eichhorn et al., 2016; Liu et al., 2019; Passmore and Coller, 2022). Oocyte meiotic maturation and early embryogenesis occur in the absence of transcription and rely on maternal mRNAs stored in oocytes (Susor et al., 2015). Defects in this process can lead to oocyte maturation arrest and early embryonic development problems.

PATL2 (PAT1 homolog 2), belonging to the PAT1 family, was first identified in *Xenopus* eggs as an oocyte-specific RNA-binding protein (Rother et al., 1992; Ozgur et al., 2010) that binds to maternal mRNA in *Xenopus* eggs and regulates its translation (Nakamura et al., 2010). We, and others, have independently identified that bi-allelic mutations in *PATL2* cause oocyte maturation arrest leading to female infertility (Chen et al., 2017; Maddirevula et al., 2017; Christou-Kent et al., 2018), and subsequent studies and case reports further confirmed this conclusion and expanded the early embryonic development arrest phenotype (Huang et al., 2018, 2022; Wu et al., 2019; Liu et al., 2020). However, the physiological function of PATL2 in the process of oocyte maturation and embryonic development is largely unknown.

In this study, we investigated the physiological function of PATL2 in oocyte maturation and embryonic development by using knockout and knock-in mouse models. We found that PATL2 coupled with CPEB1 and EIF4E to maintain mRNA stability *in vitro*, and *Patl2* knockout impaired the maternal transcriptome and the protein synthesis of maternal mRNAs, thus leading to female infertility. Furthermore, we found that phosphorylation of PATL2 residue S279 plays an important role in its degradation. This study thus shows the physiological function of PATL2 in the process of oocyte maturation and embryonic development and clarifies that PATL2 phosphorylation regulates the protein level of PATL2 for regulating the expression of maternal mRNAs.

RESULTS

Patl2 knockout in mice caused oocyte maturation defects and embryonic development arrest leading to female infertility

Previous transcriptome analyses have shown that *Patl2* mRNA is highly expressed in mouse and human oocytes (Chen et al., 2017; Christou-Kent et al., 2018). To study the physiological functions of PATL2, we generated a knockout mouse strain using the CRISPR/Cas9 system to make an 11-bp deletion in exon 1 of the *Patl2* gene (Fig. 1A). This deletion caused a reading-frame shift, and western blotting analysis confirmed that the PATL2 protein was deleted in the oocytes of *Patl2*$^{-/-}$ mice (Fig. 1B). *Patl2*$^{-/-}$ female mice were sterile, whereas the males exhibited normal fertility (Fig. 1C), and an *in vitro* maturation assay showed that the *Patl2*$^{-/-}$ female mice had significantly decreased rates of first polar body extrusion

[1]Institute of Pediatrics, Children's Hospital of Fudan University, the Institutes of Biomedical Sciences, the State Key Laboratory of Genetic Engineering, School of Life Sciences, Fudan University, Shanghai 200032, China. [2]NHC Key Lab of Reproduction Regulation (Shanghai Institute for Biomedical and Pharmaceutical Technologies), Fudan University, Shanghai 200032, China. [3]State Key Laboratory of Reproductive Medicine and Offspring Health, Department of Histology and Embryology, Nanjing Medical University, Nanjing 211166, China.
*These authors contributed equally to this work

‡Authors for correspondence (wangleiwanglei@fudan.edu.cn; sangqing@fudan.edu.cn; guo_xuejiang@njmu.edu.cn)

Z.Z., 0000-0002-4725-883X; B.C., 0000-0002-9921-2155; X.G., 0000-0002-0475-5705; Q.S., 0000-0002-9895-1394; L.W., 0000-0002-3400-0434

Handling Editor: Haruhiko Koseki
Received 3 January 2023; Accepted 9 May 2023

Development (2023) 150, dev201572. doi:10.1242/dev.201572

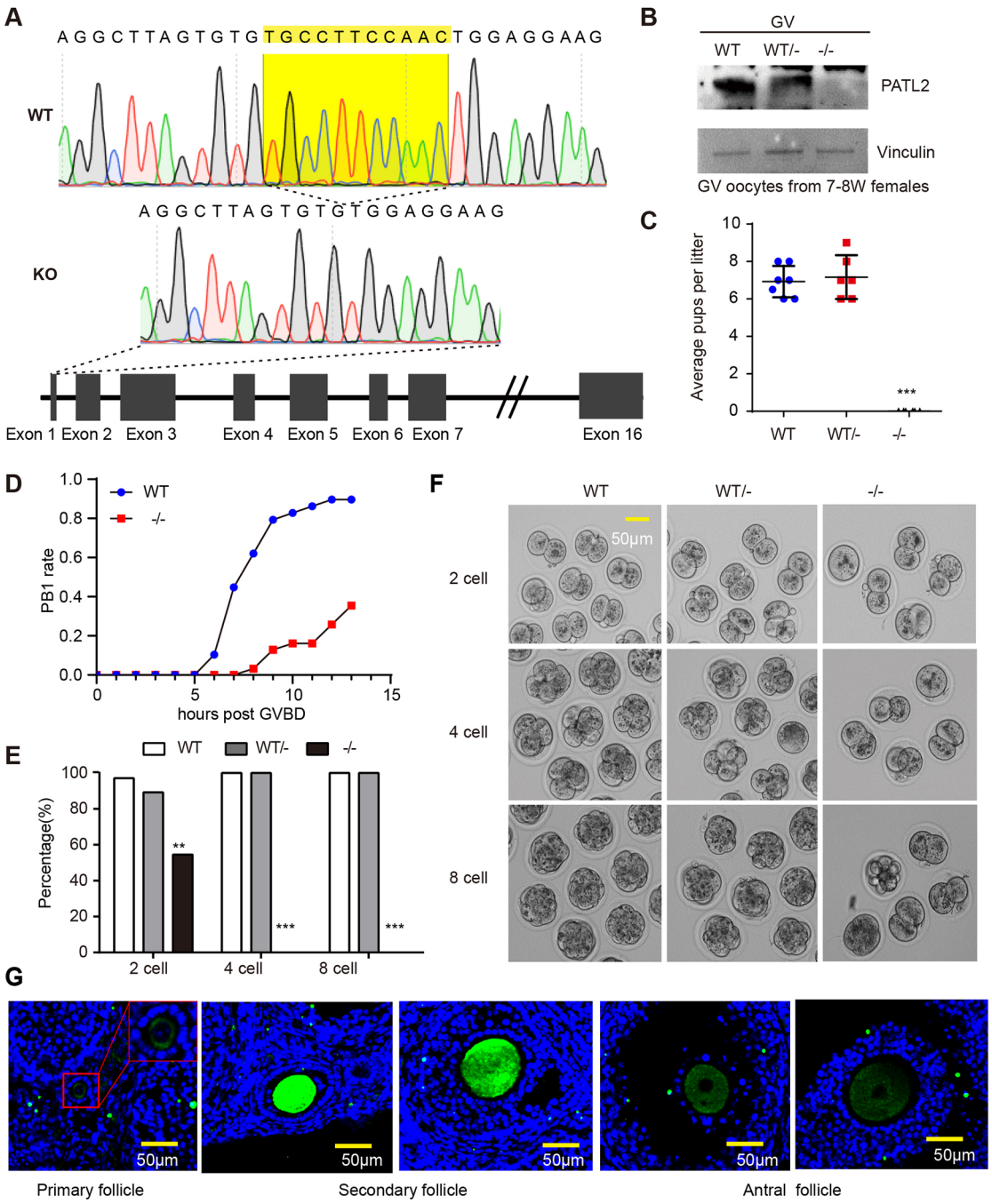

Fig. 1. *Patl2* is an oocyte-specific gene that is essential for female infertility. (A) Schematic of strategy for *Patl2* knockout mice. (B) Western blot results showing PATL2 expression in the oocytes of WT, *Patl2*$^{+/-}$ and *Patl2*$^{-/-}$ females. *n*=80. GV oocytes from 7- to 8-week-old (7-8W) females. (C) The average litter size in WT, *Patl2*$^{+/-}$ and *Patl2*$^{-/-}$ females. (D) The first polar body (PB1) rate of WT (*n*=29) and *Patl2*$^{-/-}$ (*n*=31) oocytes. (E) Developmental rates of WT (*n*=35), *Patl2*$^{+/-}$ (*n*=28) and *Patl2*$^{-/-}$ (*n*=22) embryos. (F) Representative images of embryos derived from WT, *Patl2*$^{+/-}$ and *Patl2*$^{-/-}$ females. *n*=3 mice for each genotype at each developmental stage. (G) Immunostaining analysis of PATL2 in oocytes of different follicle developmental stages. Scale bars: 50 µm.

(Fig. 1D). After *in vitro* fertilization, the metaphase II (MII) oocytes derived from ovulation stimulation in *Patl2*$^{-/-}$ female mice could be fertilized, but they all arrested at the two-cell stage, whereas the control embryos from the wild-type (WT) and *Patl2*$^{+/-}$ mice exhibited normal embryonic development (Fig. 1E,F). Immunostaining showed that PATL2 was specifically expressed in oocyte cytoplasm and that PATL2 protein level was increased in the oocytes of secondary follicles (Fig. 1G). These results confirmed the essential role of PATL2 in female infertility.

PATL2 deletion caused a reduction of the total amount of mRNA in GV oocytes

PATL2 is reported to be an oocyte-specific RNA-binding protein (Chen et al., 2017), and thus we explored the effect of PATL2 deletion on mRNA expression in the oocyte maturation process. Germinal vesicle (GV) and MII-stage oocytes were collected for RNA-seq analysis. First, we normalized the FPKM values of genes to the corresponding FPKM values of *GFP* or *mCherry* and analyzed the overall decay of maternal mRNA in WT and *Patl2*$^{-/-}$

Development (2023) 150, dev201572. doi:10.1242/dev.201572

oocytes during meiotic maturation, and we observed an obvious decrease in total mRNA copies in *Patl2*$^{-/-}$ oocytes at the GV stage compared with WT oocytes (Fig. 2A). This decrease seemed to be weakened in MII oocytes because 80% of the mRNAs were degraded during meiotic maturation (GV to MII) in WT oocytes (Fig. 2A). We confirmed the result by real-time quantitative reverse transcription PCR (qRT-PCR), with transcripts all showing significant decreases (Fig. 2B; Fig. S1A). We then proposed that deletion of PATL2 had a major effect on the decrease of mRNA expression in growing oocytes and in fully grown GV oocytes. To prove this, we collected growing oocytes from postnatal day (P)5 and P10 female mice, GV oocytes, MI and MII oocytes from 7-8-week-old female mice. We performed qRT-PCR analysis of three clearly downregulated genes, and all three genes showed the greatest decrease at the GV stage (Fig. 2C-E; Fig. S1B-D). To further confirm this, we re-performed the RNA-seq analysis of GV-stage oocytes of WT and *Patl2*$^{-/-}$ mice in five biological replicates. The results showed a significant decrease in total mRNA in *Patl2*$^{-/-}$ oocytes (Fig. 2F,G; Fig. S3). In addition, oligo(dT) *in situ* hybridization (ISH) staining also showed a significant decrease in poly(A) mRNA in *Patl2*$^{-/-}$ oocytes (Fig. 3A,B; Fig. S2A). To examine the role of transcriptional activity, we performed a

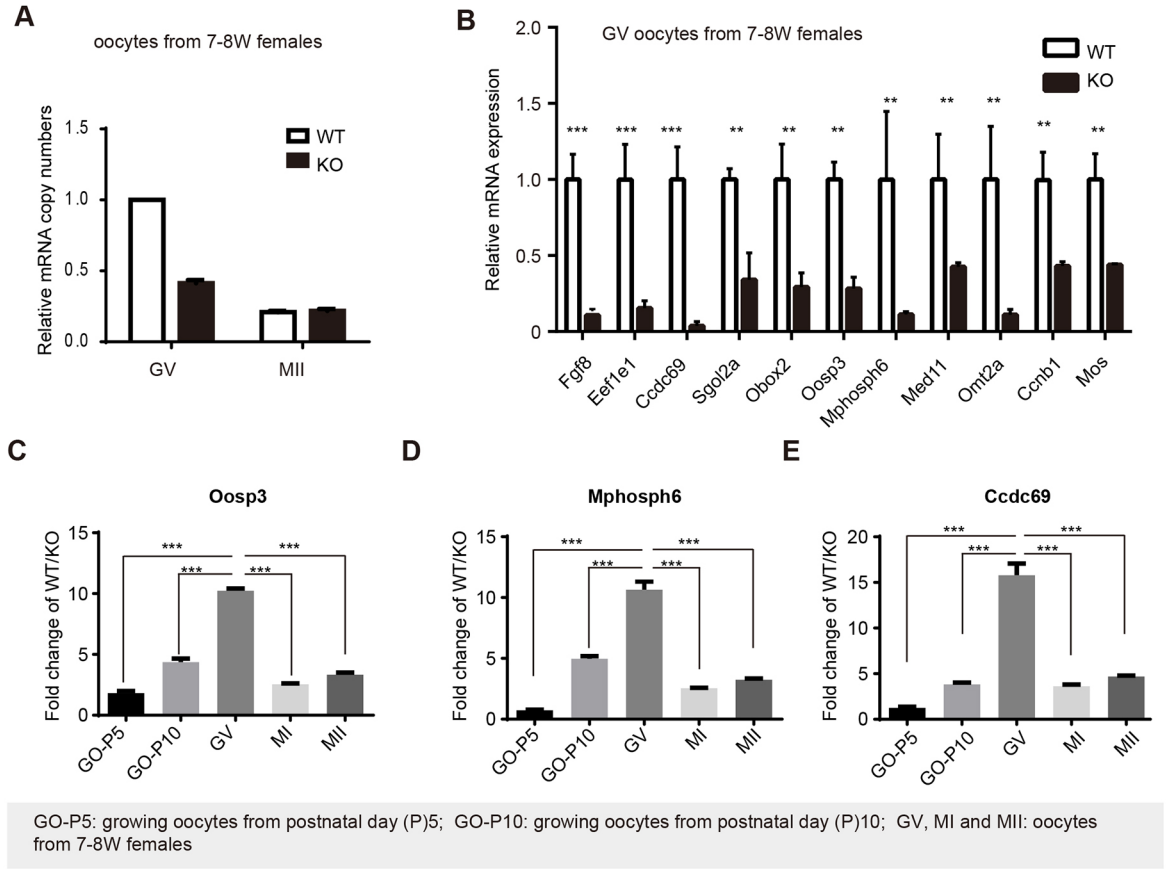

Fig. 2. PATL2 deletion led to decreased maternal mRNA in growing oocyte. (A) The relative mRNA copy number in WT and *Patl2*$^{-/-}$ (KO) samples at the GV and MII stages using 30 oocytes for each stage and each genotype pooled for one sample, the replicates were: WT-GV (*n*=1); KO-GV (*n*=2); MII-WT (*n*=2); MII-KO (*n*=2). (B) qRT-PCR confirming that the relative levels of the indicated transcripts decreased in GV oocytes. (C-E) qRT-PCR analysis of three representative transcripts in growing oocytes from P5, P10 and GV, MI and MII oocytes. (F) Heat map of Spearman correlation coefficients among WT and *Patl2*$^{-/-}$ oocytes (*N*=5). (G) The relative mRNA copy-number in WT and *Patl2*$^{-/-}$ GV oocytes with five biological replicates. GV oocytes from 7- to 8-week-old (7-8W) females. Data are mean±s.d. *P<0.05, **P<0.01, ***P<0.001 (two-tailed unpaired Student's *t*-test).

Development (2023) 150, dev201572. doi:10.1242/dev.201572

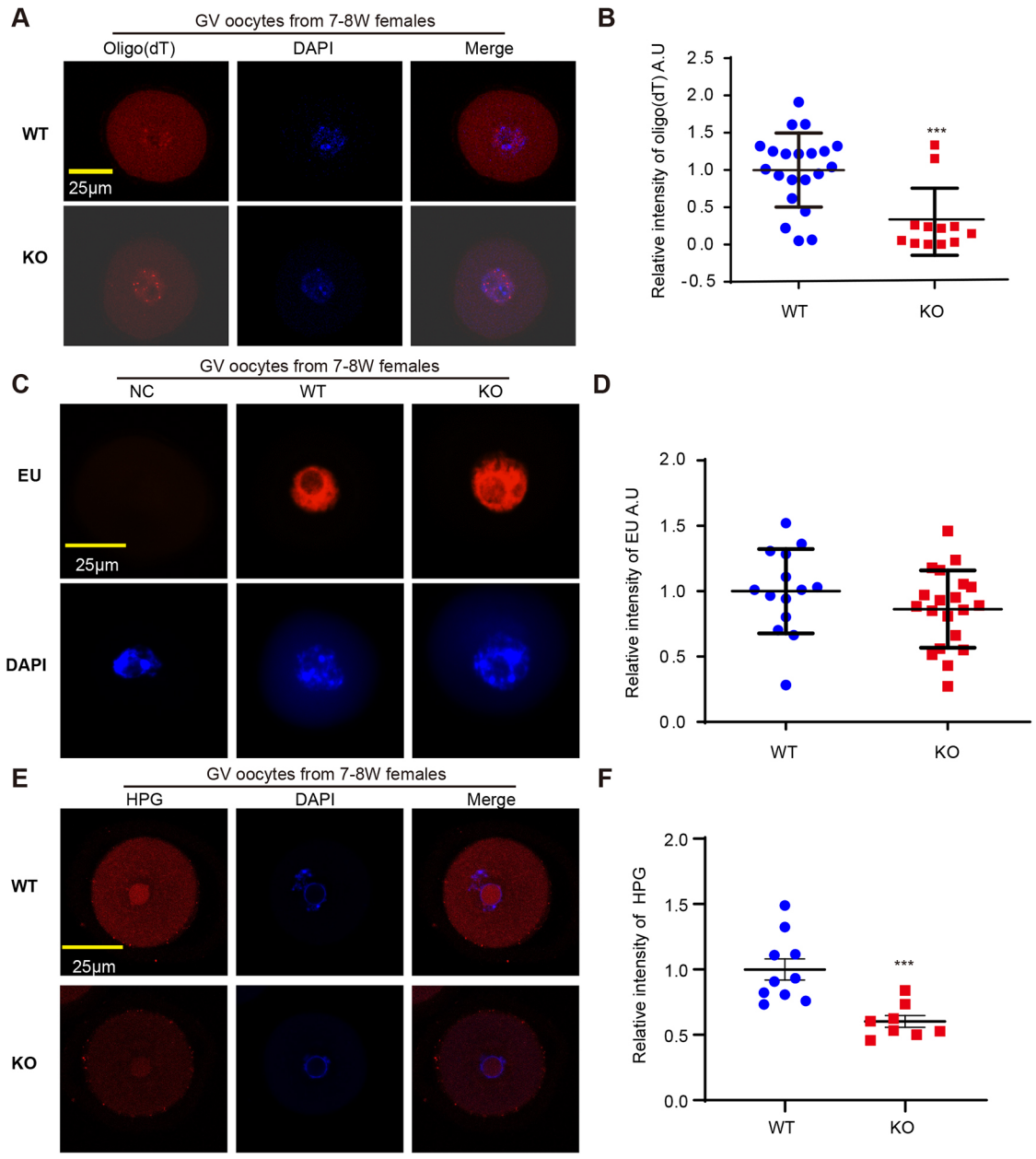

Fig. 3. PATL2 was required for maternal mRNA expression in oocytes with little effect on transcription activity. (A) Poly(A) mRNA was decreased in *Patl2*$^{-/-}$ GV oocytes as measured by oligo(dT) *in situ* hybridization. WT (*n*=21), *Patl2*$^{-/-}$ (*n*=12). (B) The quantification of oligo(dT) intensity. (C) EU transcription activity analysis in WT (*n*=14) and *Patl2*$^{-/-}$ (*n*=20) oocytes. (D) The EU intensity quantification analysis. (E) HPG staining showed decreased protein synthesis in *Patl2*$^{-/-}$ oocytes. WT (*n*=10), *Patl2*$^{-/-}$ (*n*=8). (F) Quantitative analysis of E. GV oocytes from 7- to 8-week-old (7-8W) females. Data are mean±s.d. ***P<0.001 (two-tailed unpaired Student's *t*-test). Scale bars: 25 μm.

5-ethynyl uridine (EU) staining experiment, and the results showed that there was no significant difference between WT and *Patl2*$^{-/-}$ oocytes (Fig. 3C,D; Fig. S2B). The mRNA transporting assay showed that the cRNA in *Patl2*$^{-/-}$ GV oocyte nucleus could transport to cytoplasm normally, as in WT oocytes, at 30 min and 60 min after nucleus cRNA injection (Fig. S4). We then analyzed protein synthesis in the WT and *Patl2*$^{-/-}$ oocytes according to the L-homopropargylglycine (HPG) assay, which showed that the protein synthesis in *Patl2*$^{-/-}$ oocytes decreased significantly (Fig. 3E,F). Together, these results demonstrate that PATL2 deletion leads to the decrease of maternal mRNA expression in GV stages.

PATL2 couples CPEB1 and EIF4E to maintain mRNA stability *in vitro*

Our study showed that PATL2 is an oocyte-specific RNA binding protein and is indispensable for maternal mRNA expression in GV oocytes. Previous studies have suggested that PATL2 might interact with CPEB1, DDX6 and EIF4E, which are typical RNA-binding proteins involved in oocyte mRNA stability in *Xenopus* and mice (Stebbins-Boaz et al., 1999). To confirm this, we co-expressed PATL2 with CPEB1, DDX6 and EIF4E in HeLa cells and performed a co-immunoprecipitation assay. The results showed that PATL2 co-interacted with EIF4E and CPEB1 independent of RNA (Fig. 4A,B) and that endogenous PATL2 in mouse ovaries

Development (2023) 150, dev201572. doi:10.1242/dev.201572

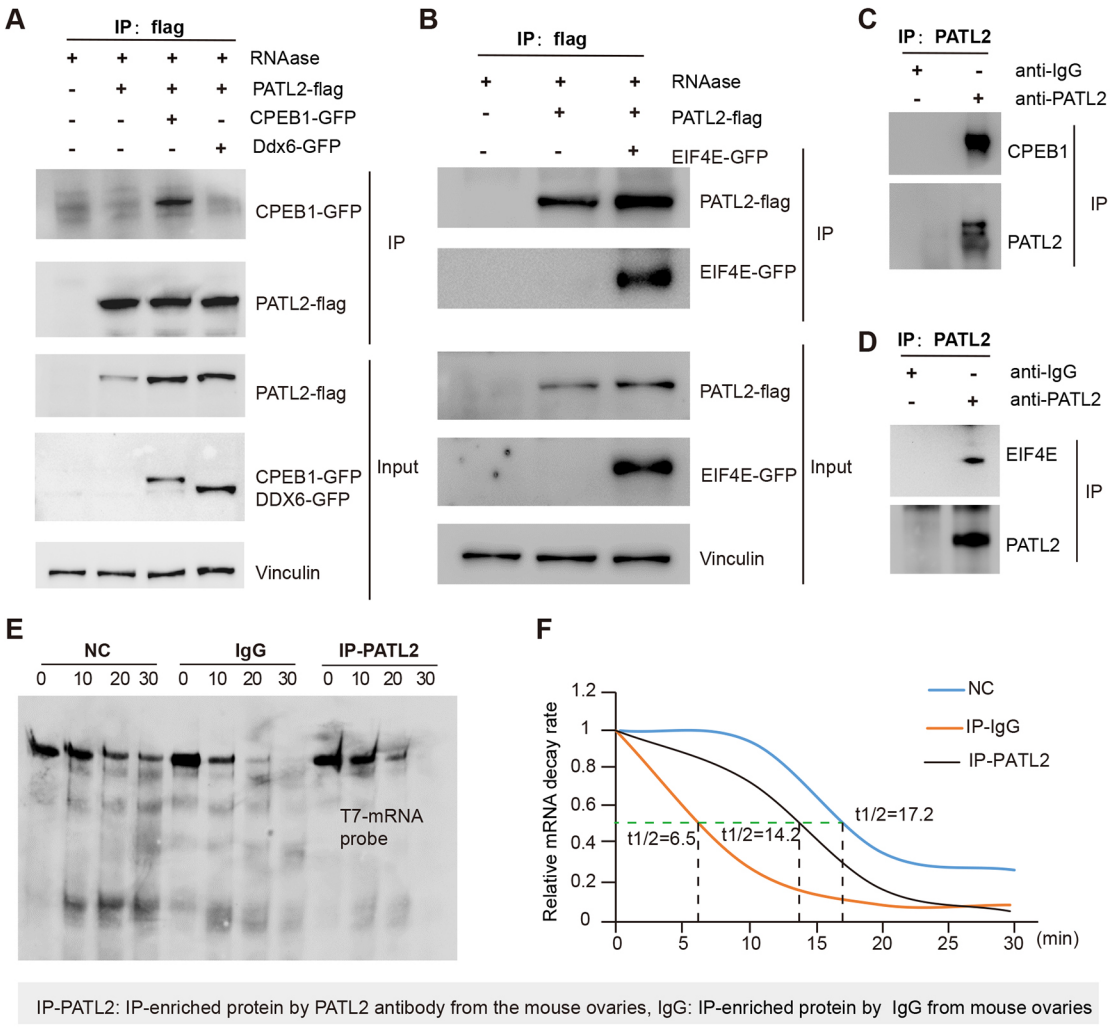

IP-PATL2: IP-enriched protein by PATL2 antibody from the mouse ovaries, IgG: IP-enriched protein by IgG from mouse ovaries

Fig. 4. PATL2 coupled CPEB1 and EIF4E to maintain mRNA stability *in vitro*. (A) PATL2 interacted with CPEB1 independent of RNA in cultured HeLa cells. (B) PATL2 interacted with EIF4E independent of RNA in cultured HeLa cells. (C) PATL2 interacted with CPEB1 in ovary lysates. (D) PATL2 interacted with EIF4E in ovary lysates. (E) The RNA decay assay with NC (free water), IgG and IP-PATL2. (F) The effect of NC, IgG and IP-PATL2 on the half-life of the RNA probe. IP-PATL2, IP-enriched protein by PATL2 antibody from the mouse ovaries; IgG, IP-enriched protein by IgG from mouse ovaries.

bound to both CPEB1 and EIF4E (Fig. 4C,D). To explore the effect of the PATL2 on mRNA stability, an RNA decay assay was performed. The RNA probe was incubated with IP-enriched protein by PATL2 antibody and IgG *in vitro*. The results indicated that the IP-enriched protein (including CPEB1 and EIF4E) by PATL2 antibody from the mouse ovaries significantly increased the RNA half-life compared with the IgG control, suggesting that PATL2 plays a role in maintaining mRNA stability (Fig. 4E,F). These results suggested that PATL2 might couple CPEB1 and EIF4E to maintain mRNA stability.

PATL2 phosphorylation at S279 over the course of oocyte maturation

Western blots of PATL2 at the GV, MI and MII stage showed a decreasing protein level of PATL2 when entering MI, and the electrophoresis band in MI oocytes appeared to shift to a greater molecular weight compared with GV oocytes (Fig. 5A,B). Thus, we speculated that PATL2 phosphorylation might be occurring after germinal vesicle breakdown (GVBD). To verify this hypothesis, we treated the MI oocyte lysates with λ-PPase, an Mn^{2+}-dependent protein phosphatase that can remove the phosphorylation of serine, threonine, tyrosine and histidine residues. Western blot showed that λ-PPase treatment significantly decreased the protein level of PATL2 and p-ERK1/2 (a positive control) in MI oocytes compared with untreated MI oocytes (Fig. 5C-E). To further confirm the phosphorylation of PATL2 after GVBD, we compared the phosphorylation level between GV and MI oocytes using a Phos-Ser antibody. The results showed an obvious phosphorylation band in MI oocytes compared with GV oocytes (Fig. 5F). Together, these results showed that PATL2 was phosphorylated and degraded during the process of oocyte maturation. Next, we sought to determine the phosphorylation site of PATL2. We ectopically expressed PATL2 in HeLa cells and performed phosphorylation proteomics (Fig. 5G,H). We identified S279 as a phosphorylation site in PATL2 (Fig. 5I; Fig. S5; Table S4), and this amino acid is highly conserved across humans, chimps, mice, pigs, horses and dogs (Fig. 5I).

S279 phosphorylation degraded PATL2 via the ubiquitin-mediated pathway

To determine the function of the phosphorylation of PATL2, we generated the S279D phosphomimetic mutant. We first confirmed

Development (2023) 150, dev201572. doi:10.1242/dev.201572

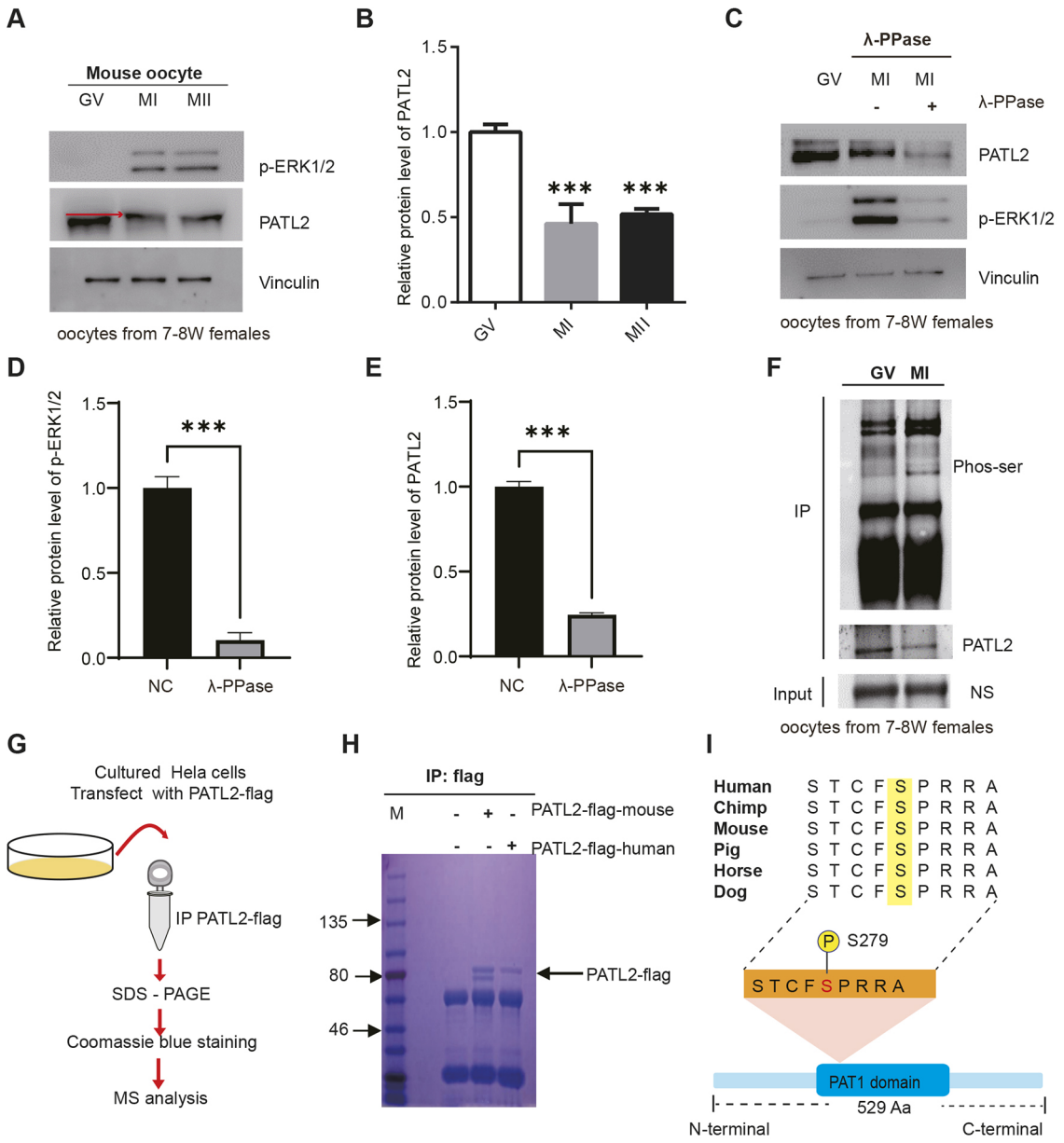

Fig. 5. PATL2 phosphorylation at S279 over the course of oocyte maturation. (A) The protein levels of PATL2 and P-ERK1/2 in GV, MI and MII oocytes. The red arrow indicates a shift of the PATL2 band when entering the MI stage. *n*=80. (B) Quantitative analysis of PATL2 in GV, MI and MII stages. oocytes from 7- to 8-week-old (7-8W) females. (C) Protein levels of PATL2 and P-ERK1/2 in MI oocytes after λ-PPase treatment. *n*=80. (D) Quantitative analysis of PATL2 with or without λ-PPase treatment. (E) Quantitative analysis of P-ERK1/2 with or without λ-PPase treatment. (F) The Phos-Ser antibody confirmed the phosphorylation of PATL2 in MI oocytes. *n*=200. (G) Schematic showing phosphoproteomics in cultured HeLa cells with PATL2 overexpression. (H) Coomassie Brilliant Blue staining of PATL2 in cultured HeLa cells, with the black arrow indicating the PATL2 band. (I) The S279 phosphorylation site is conserved among different species. Data are mean±s.d. ***P<0.001 (two-tailed unpaired Student's *t*-test).

that the S279D mutation had no effect on the PATL2 protein level in HeLa cells (Fig. 6A,B). We next injected WT and S279D cRNA into GV oocytes, and the western blotting assay indicated that the S279D mutation caused a sharp decrease in the PATL2 protein level in oocytes (Fig. 6C,D). In addition, PATL2 was sensitive to MG132, an inhibitor of the proteasome degradation (Fig. S6A,B), and thus we proposed that the S279D phosphomimetic mutant may affect the ubiquitin (Ub)-mediated degradation of PATL2. We found that the S279D mutation promoted the polyubiquitylation of PATL2 (Fig. 6E; Fig. S6C). All of these results indicate that phosphorylation of S279 promoted Ub-mediated degradation of PATL2.

The S279 phosphorylation state controls the function of PATL2 *in vivo*

To determine the function of the phosphorylation of PATL2 *in vivo*, we generated the $PATL2^{S279D}$ knock-in mouse model using the CRISPR/Cas9 system (Fig. 7A). There were significantly fewer pups per litter in $Patl2^{S279D/S279D}$ mice compared with $Patl2^{WT/S279D}$ mice, indicating reduced fertility (Fig. 7B), whereas the male mice exhibited normal fertility. After *in vitro* fertilization, the zygotes from $Patl2^{S279D/S279D}$ mice showed decreased rates of two cell, four- to eight-cell, morula and blastocyst stages compared with $Patl2^{WT/S279D}$ mice (Fig. 7C,D). We then measured the protein level of PATL2 in the oocytes of $PATL2^{WT/S279D}$ and

Development (2023) 150, dev201572. doi:10.1242/dev.201572

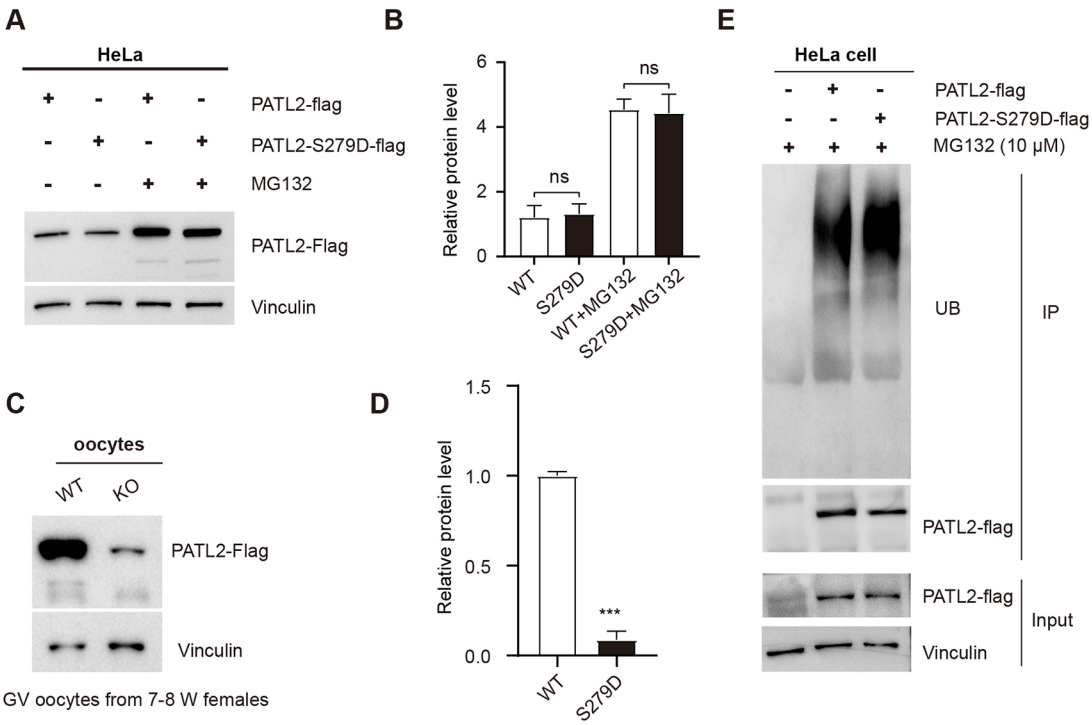

Fig. 6. The S279D mutation promoted the Ub-mediated protein degradation of PATL2. (A) The effect of the S279D mutation on the protein level in cultured HeLa cells with or without MG132. (B) Quantitative analysis of A. (C) Protein level of S279D decreased sharply compared with WT in cRNA-injected oocytes. *n*=50. GV oocytes from 7- to 8-week-old (7-8W) females. (D) Quantitative analysis of C. (E) The S279D mutation promoted the Ub-mediated protein degradation of PATL2 in cultured HeLa cells. Data are mean±s.d. ***P<0.001 (two-tailed unpaired Student's *t*-test). ns, not significant.

PATL2$^{S279D/S279D}$ mice. Similar to the *in vitro* result, the protein level of PATL2 in the oocytes of *PATL2*$^{S279D/S279D}$ mice was sharply decreased (Fig. 7E,F), whereas the PATL2 mRNA level showed no obvious difference (Fig. 7G). Considering that the Oligo(dT) ISH showed similar weaker poly(A) probe binding in *Patl2*$^{S279D/S279D}$ GV oocytes than in control mice, this indicated that a reduction of poly(A) mRNA may also happen (Fig. 7H,I). The EU staining showed no significant difference in transcriptional activity between *Patl2*$^{WT/S279D}$ and *Patl2*$^{S279D/S279D}$ mice (Fig. S7). Protein synthesis in *Patl2*$^{S279D/S279D}$ oocytes also decreased significantly (Fig. 7J,K). These results indicated that phosphorylation of PATL2 was essential for its function *in vivo*.

Our work revealed the unrecognized roles of PATL2 in regulating the maternal transcriptome by recruiting CPEB1 and EIF4E in oocytes. Furthermore, we showed the essential role of PATL2 phosphorylation in oocyte maturation using *Patl2*$^{S279D/S279D}$ knock-in mice, and we illustrated the mechanism through which PATL2 regulates its protein level via ubiquitin-mediated proteasomal degradation (Fig. 8).

DISCUSSION

The accumulation and storage of maternal mRNA is essential for oocyte maturation and embryonic development (Sha et al., 2020). To maintain the translationally silenced state, the lengths of the poly(A) tails of maternal mRNAs are shortened and the mRNAs are sequestered into cytoplasmic granules (Racki and Richter, 2006; Liu et al., 2022; Passmore and Coller, 2022). These shorter poly(A) tails present a big challenge for mRNA stability in the GV arrested stage. To maintain mRNA stability, P-bodies disappear during oocyte growth, and the factors related to mRNA decay are highly limited (Swetloff et al., 2009). For example, the decapping factors DCP1 and DCP2 and the deadenylating factor BTG4 are almost completely absent in GV stage (Ma et al., 2013; Yu et al., 2016). However, these mechanisms alone are not sufficient. In this study, we showed that PATL2 is highly expressed before GVBD and might be coupled with EIF4E and CPEB1 to regulate maternal mRNA expression in immature oocytes.

PATL2 belongs to the PAT1 family, and the PAT1 RNA-binding proteins are highly conserved from fungi to humans (Marnef et al., 2010; Marnef and Standart, 2010). Vertebrates have two paralog proteins, including PAT1A (PATL2), which is expressed in oocytes, and PAT1B (PATL1), which is expressed in embryos and somatic cells (Marnef et al., 2010). In cultured cells, PATL1 is reported to function in cytoplasmic mRNA decay by physically connecting deadenylation with decapping and by controlling the assembly of processing bodies (Ozgur et al., 2010). However, PATL2 seems to have little effect on RNA decay in cultured cells (Ozgur et al., 2010). Combined with previous genetic studies (Chen et al., 2017; Maddirevula et al., 2017; Christou-Kent et al., 2018), all these findings indicate that PATL2 might play a specific role in oocytes. A previously reported *Patl2* knockout mouse model showed using Affymetrix arrays that PATL2 deletion causes the downregulation of a set of highly relevant genes involved in oocyte maturation and early embryonic development, thus leading to subfertility (Christou-Kent et al., 2018). However, the role of PATL2 in oocyte maturation has not been fully investigated. Our study used spiked-in transcriptome analysis and oligo (dT) ISH to show that PATL2 deletion caused the global decay of poly(A) mRNA in immature oocytes leading to female sterility. The level of decay increased following oocyte growth and reached its highest in GV stages, after which it slowed through the MI and MII stages. In eukaryotes, mRNA homeostasis begins with precursor messenger RNA (pre-mRNA) transcription and processing into mature mRNA in the nucleus. The mRNA is subsequently recognized and

Development (2023) 150, dev201572. doi:10.1242/dev.201572

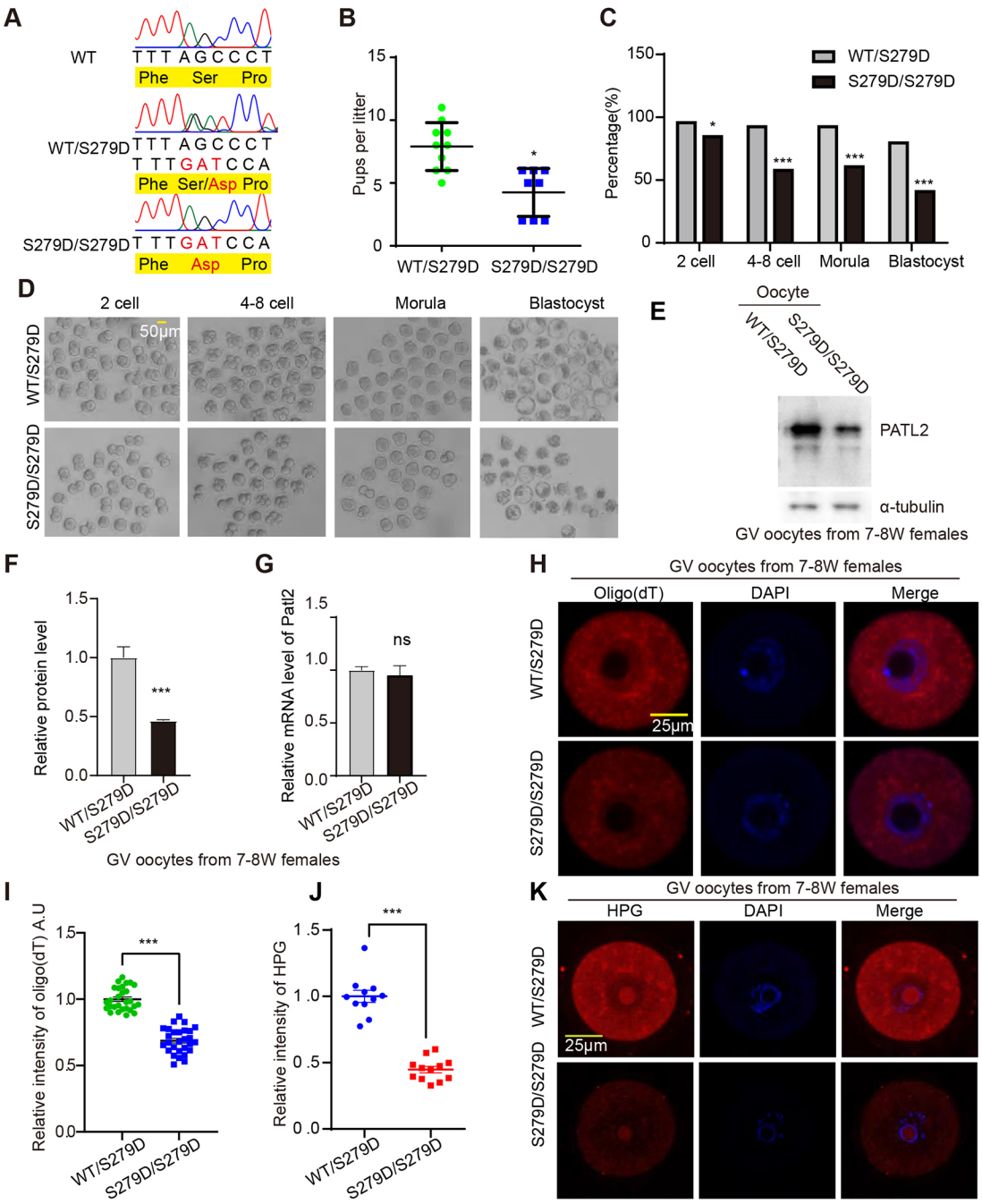

Fig. 7. The S279D mutation caused reduced female fertility with decreased poly(A) mRNA in GV oocytes. (A) Genotyping of S279D mice confirmed by Sanger sequencing. (B) The average litter size of the *Patl2*$^{WT/S279D}$ and *Patl2*$^{S279D/S279D}$ female mice. (C) The development rate of *Patl2*$^{WT/S279D}$ (*n*=93) and *Patl2*$^{S279D/S279D}$ (*n*=71) embryos at the two-cell, four- to eight-cell, morula and blastocyst stages. (D) Representative images of *Patl2*$^{WT/S279D}$ (*n*=93) and *Patl2*$^{S279D/S279D}$ (*n*=71) embryos at the two-cell, four- to eight-cell, morula and blastocyst stage. (E) The PATL2 protein level in *Patl2*$^{S279D/S279D}$ oocytes was significantly decreased compared with *Patl2*$^{WT/S279D}$ oocytes. *n*=80. (F) Quantitative analysis of E. (G) The mRNA level of *Patl2* in the oocytes of *Patl2*$^{S279D/S279D}$ and *Patl2*$^{WT/S279D}$ mice. (H) Oligo(dT) ISH in *Patl2*$^{WT/S279D}$ (*n*=28) and *Patl2*$^{S279D/S279D}$ (*n*=28) oocytes. (I) Intensity analysis of the oligo(dT) probe. (J) Intensity analysis of HPG in *Patl2*$^{WT/S279D}$ (*n*=11) and *Patl2*$^{S279D/S279D}$ (*n*=12) oocytes. (K) HPG staining showed decreased protein synthesis in *Patl2*$^{S279D/S279D}$ oocytes. GV oocytes from 7- to 8-week-old (7-8W) females. Data are mean±s.d. *P<0.05, ***P<0.001 (two-tailed unpaired Student's *t*-test). ns, not significant. Scale bars: 50 μm (D); 25 μm (H,K).

packaged by proteins into an mRNA ribonucleoprotein complex (mRNP) and exported to the cytoplasm for translation and degradation (Kang and Han, 2011). In this study, we found a reduction of total mRNA in KO oocytes. EU staining and an RNA transporting assay showed that PATL2 knockout had little effect on transcription and mRNA transporting. As PATL2 mainly localized in oocyte cytoplasm and had little signal in the nucleus, it was thought that PATL2 might function by affecting the stability of mRNA. However, an alternative possibility was that there was a difference in the amount of mRNA packaged in WT and knockouts in earlier stages of growing follicles. This demonstrated that PATL2 may be an oocyte-specific mRNA stability-maintaining protein

Development (2023) 150, dev201572. doi:10.1242/dev.201572

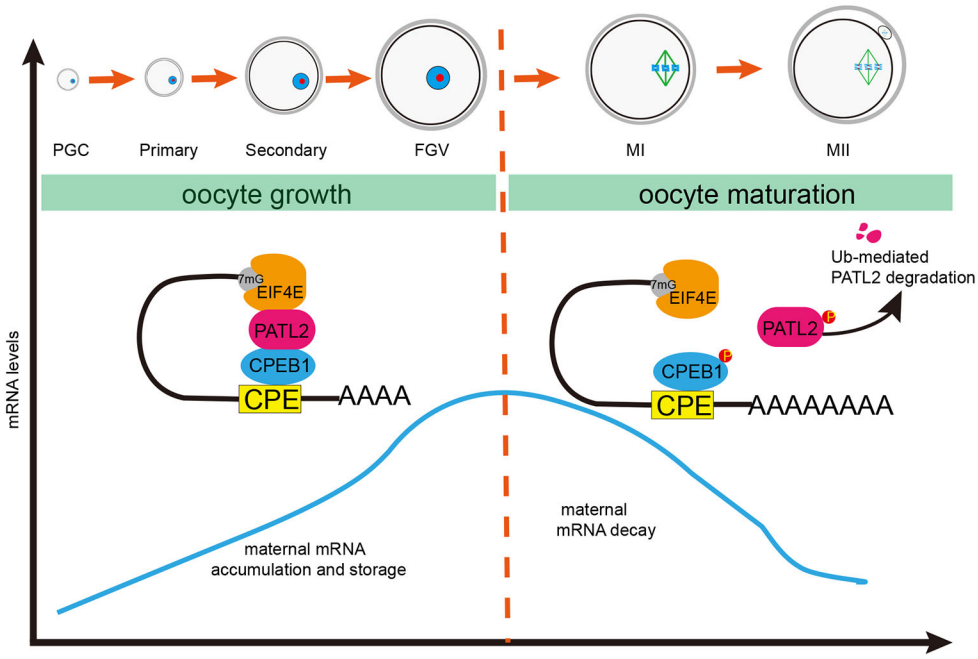

Fig. 8. Summary of PATL2 function in regulating maternal mRNA expression in growing oocytes. Maternal mRNA accumulates and is stored in the oocyte cytoplasm with short poly(A) tails. PATL2 may function as an adaptor protein to recruit EIF4E and CPEB1 to maintain the stability of mRNA in growing oocytes. In the oocyte maturation process, PATL2 is phosphorylated at S279 and subsequently degraded by Ub-mediated protein degradation. EIF4E and CPEB1 are then released and CPEB1 phosphorylation activates polyadenylation and translation.

during the oocyte growth process. The major effect of maternal mRNA in the GV stage might partly explain the GV arrests phenotype of human mutations. The phenotypic heterogeneity between humans and mice might be due to the following reasons. First, the inherent differences in fertility between humans and mice might have led the mice to exhibit a weaker phenotype. Second, among reported cases with *PATL2* variants, a portion of them also caused early embryo development arrest, which might be due to the dose effect of the variants (Ma et al., 2013; Chen et al., 2017; Maddirevula et al., 2017; Christou-Kent et al., 2018; Huang et al., 2018, 2022; Liu et al., 2020). However, this needs to be further confirmed by research on oocytes in *PATL2* variants.

In immature oocytes, messenger RNAs containing a cytoplasmic polyadenylation element (CPE) are translationally dormant (masked). In *Xenopus*, maternal mRNA is incorporated in a complex containing CPE-binding protein (CPEB), maskin and EIF4E (Stebbins-Boaz et al., 1999; Groisman et al., 2001; Minshall et al., 2007). However, TACC3, the homologous analog of maskin in mammals, appears to function as a spindle assembly protein in mouse and human oocytes rather than an RNA-binding protein (Ding et al., 2017; So et al., 2019; Wu et al., 2022). Here, we showed that PATL2 might substitute for the role of maskin as an adaptor protein to recruit EIF4E and CPEB1. PATL2 interacted with EIF4E and CPEB1 to maintain mRNA stability in immature oocytes (Fig. 8).

The translational activation of stored maternal mRNAs depends on the regulation of phosphorylation upon meiotic resumption (Stebbins-Boaz et al., 1996; Mendez et al., 2002; Setoyama et al., 2007; Sha et al., 2017). Once maturation begins, newly phosphorylated CPEB recruits the cleavage and polyadenylation specificity factor (CPSF) and poly(A) polymerase (PAP), which together function to elongate the poly(A) tail (Kang and Han, 2011; Clerici et al., 2018). Here, we showed that the RNA binding protein PATL2 is highly phosphorylated, and we showed that phosphorylation occurs at residue S279 upon meiotic resumption. In addition, we showed the essential role of PATL2 phosphorylation using *Patl2*$^{S279D/S279D}$ knock-in mice, and we found that PATL2 regulates its protein level via ubiquitin-mediated proteasomal degradation (Fig. 8). The S279D mutant affected the protein levels in oocytes and had no effect in HeLa cells. This may be because: PATL2 is an oocyte-specific RNA binding protein and had no expression in HeLa cells, so the ectopic expression in HeLa cells might not mimic the situation in oocytes; the protein post-translational modification level (such as phosphorylation level and ubiquitylation modifications) might be different in HeLa cells and oocytes, and the HeLa cell might increase the phosphorylation level and ubiquitination modifications to clean up the ectopic expression of PATL2; or other factors specifically expressed in oocytes might also be involved in regulation of PATL2 protein level.

In this study, we confirmed the essential role of PATL2 in oocyte growth and oocyte maturation, demonstrated the effect of PATL2 on mRNA expression, and clarified the phosphorylation modification of PATL2. Our work thus sheds light on the novel mechanism of PATL2-related maternal mRNA storage and post-translational modifications in oocytes.

MATERIALS AND METHODS

Plasmid construction and expression in HeLa cells

The full-length coding sequences of PATL2, CPEB1, EIF4E and DDX6 were amplified and cloned into the pCMV6 vector fusing with a C-terminal FLAG or GFP tag to obtain PATL2-FLAG, CPEB1-GFP, EIF4E-GFP and DDX6-GFP. The KOD-Plus Mutagenesis Kit (Toyobo) was used to introduce the S279D (AGC>GAT) mutant. The HeLa cell line was obtained from the Cell Bank of the Shanghai Institute for Biological Sciences, the Chinese Academy of Sciences (Shanghai, China). HeLa cells were cultured in Dulbecco's modified Eagle's medium (DMEM) supplemented with 10% fetal bovine serum and 1% penicillin-streptomycin (Gibco) at 37°C in an atmosphere of 5% CO_2. Cells were plated 24 h before transfection and maintained until the cell density reached 70-80% confluence. Before transfection, fresh complete culture medium containing serum and antibiotics was added to each well. Cell transfection was then performed using the PolyJet *In Vitro* DNA Transfection Reagent (SignaGen) according to standard protocols.

Generation of *Patl2* knockout and knock-in mice and fertility tests

The *Patl2* knockout mouse model (C57BL/6J) was generated by CRISPR/Cas-mediated genome engineering. For the *Patl2* knockout mice, a region of 11 bp in exon 1 was deleted, which caused a frameshift of coding region. For

Development (2023) 150, dev201572. doi:10.1242/dev.201572

the *Patl2* knock-in mice, the p.S279D (AGC to GAT) variant site in the donor oligonucleotide was introduced by homology-directed repair. F0 founder animals were identified by PCR followed by sequence analysis and were bred with WT mice to get the F1 generation. WT and homozygous knockout and knock-in mice (6-8 weeks) were mated with C57BL/6J WT male mice at 10-12 weeks of age for three months. The vaginal plugs were checked to confirm successful mating. The number of litters and pups per litter were calculated. Genotyping primers used in this study are shown in Table S1.

Mouse oocyte collection, cRNA transcription and microinjection

GV oocytes were collected from ovaries of the 7- to 8-week-old female Institute of Cancer Research mice (Beijing Vital River Laboratory Animal Technology) by puncturing the antral follicles with a fine needle under the dissecting microscope, and the GV oocytes were cultured in M2 medium (Sigma-Aldrich). WT and mutant plasmids were linearized by digestion with the AgeI restriction enzyme (R0552S, New England Biolabs), and 1 µg of the linearized DNA was used as a template to transcribe cRNA with poly(A) tailing using the HiScribe T7 ARCA mRNA Kit (E2060S, New England Biolabs). cRNAs were then purified with the RNeasy MinElute Cleanup Kit (74204, Qiagen). For detailed microinjection methods refer to Sang et al. (2019).

Identification of the phosphorylation site of PATL2 by phosphoproteomics

HeLa cells ectopically expressing PATL2 were harvested at 36 h after transfection. Sodium dodecyl sulfate polyacrylamide gel electrophoresis (SDS-PAGE) was performed, and we stained the polyacrylamide gel with Coomassie Brilliant Blue. The overexpressed band of PATL2 was cut out and collected, and phosphoproteomics was performed as previously described (Wang et al., 2017). Briefly, tandem mass tag-labeled phosphopeptides were enriched through immobilized metal affinity chromatography and consecutive titanium dioxide methods. Raw files were searched against the mouse protein sequences obtained from the Universal Protein Resource database using the MaxQuant software (version 1.3.0.5) (Cox and Mann, 2008). The Phospho (STY) site is shown in Table S7.

Western blotting

HeLa cells were harvested after transfection for 36 h with or without MG132 and washed with phosphate-buffered saline (PBS). They were then lysed in 1× SDS loading buffer (Shanghai Wei AO Biological Technology) and boiled for 10 min for denaturation. Mouse oocytes were denatured by boiling for 10 min in 1× SDS loading buffer. Equal amounts of protein were resolved on 10% SDS-PAGE gels and transferred to nitrocellulose filter membranes. Membranes were blocked in 5% non-fat milk for 1 h and incubated with the following primary antibodies overnight at 4°C: rabbit anti-PATL2 (Abclonal; 1:500), rabbit anti-GFP (Abclonal; 1:3000), rabbit anti-Vinculin (13901; Cell Signaling Technology; 1:1000) and α-Tubulin (Sigma-Aldrich; 1:1000). Goat anti-mouse or anti-rabbit IgG (Abmart; 1:3000) was used as the secondary antibody to detect the primary antibodies. The blots were captured using ECL Western Blotting Substrate (Tanon). Antibodies used in this study are shown in Table S2.

Immunofluorescent staining

Oocytes were fixed with 2% paraformaldehyde (PFA; Sangon Biotech) for 30 min at room temperature and permeabilized in 0.5% Triton X-100 in PBS for 20 min. Oocytes were blocked in blocking buffer (3% bovine serum albumin, 0.1% Tween 20, and 0.01% Triton X-100 in PBS) for 1 h at room temperature, and all antibody incubations were performed in blocking buffer. Anti-PATL2 antibody (Abclonal; 1:100) was added for 1 h at 37°C to determine PATL2 localization. Hoechst 33342 (BD Biosciences; 1:1000) was used to label DNA for 15 min at room temperature. All images were captured on an LSM 880 laser scanning confocal microscopy (Zeiss).

Co-immunoprecipitation

PATL2-FLAG and mutant plasmids were co-transfected with the CPEB1-GFP, EIF4E-GFP and DDX6-GFP plasmid into HeLa cells. At 36 h after transfection, cell proteins were extracted with NP-40 lysis buffer (50 mM Tris, 150 mM NaCl, 0.5% NP-40, pH 7.5) containing 1% protease inhibitor cocktail (Bimake) and 50 µg/ml RNase A to digest the RNA. Total protein was incubated with anti-FLAG beads (Bimake) at 4°C for 3 h. The beads were washed with lysis buffer with 10 µg/ml RNase A three times and then boiled with SDS loading buffer for western blotting with anti-FLAG (1:3000) and anti-GFP (1:3000) antibodies.

In vitro fertilization

The 7- to 8-week-old female mice were superovulated by injecting 10 IU of pregnant mare serum gonadotropin (PMSG, Ningbo Second Hormone Factory) followed by 10 IU of human chorionic gonadotropin (hCG, Ningbo Second Hormone Factory) 46-48 h later. After 12 h, sperm were collected from the cauda epididymis of male mice and capacitated in a drop of Human Tubal Fluid (HTF) at 37°C with 5% CO_2 for 1 h. Superovulated oocytes were transferred into a new HTF drop containing capacitated sperm for fertilization at 37°C in 5% CO_2 for 6 h. Subsequently, 2 pronuclear (2PN) zygotes were selected and transferred into KSOM medium (EasyCheck, M1430) at 37°C in 5% CO_2 for blastocyst culture.

qRT-PCR

Total RNA from mouse ovaries was extracted using a RNeasy Mini Kit (Qiagen). Genomic DNA was depleted, and RNA reverse transcription was used to obtain cDNA using a PrimeScript RT reagent Kit with gDNA Eraser (TaKaRa). qRT-PCR was performed using a Quant Studio 6 Flex Real-time system with TaKaRa TB Green Premix Ex Taq (Tli RnaseH Plus). Three repeated reactions were performed for each sample. The PCR reactions were performed as follows: 95°C for 2 min and 40 cycles of 95°C for 1 s and 60°C for 30 s. The relative expression level equals $k.2^{-\Delta Ct}$ where ΔCt=Ct (*Patl2*) – Ct (*Actin*) and k is a constant (Pfaffl, 2001). All primers used in this study for qPCR are shown in Table S1.

RNA decay assay

The 200 nt Biotin-labeled-T7 probe was transcribed using a HiScribe T7 High Yield RNA Synthesis Kit (E2040) with a supplement of Bio-11-UTP (AM8450). The negative control (NC, free water), IgG (proteins immunoprecipitation from the ovary by IgG) and IP-PATL2 (proteins immunoprecipitation from the ovary by anti-PATL2 antibody) was adjusted to 11 µl using *in vitro* RNA decay buffer [50 mM HEPES-NaOH (pH 8.0), 150 mM NaCl, 2 mM $MgCl_2$, 10% glycerol, 1 mM DTT, and 1% protease inhibitors]. Then 1 µl (1000 ng) of T7 probe was incubated with NC, IgG or IP-PATL2 for 0 min, 10 min, 20 min and 30 min at 30°C. Reactions were stopped by the addition of 12 µl RNA loading buffer (95% formamide, 0.025% bromophenol blue, 0.025% xylene cyanol FF, 0.025% SDS and 5 mM EDTA) supplemented with 1 µl (400 U) RNA inhibitor. The mixture was then digested by 5 µg/ml protease K for 2 h at 65°C. Reaction products were heated for 3 min at 85°C and analyzed by 12% denaturing SDS-PAGE containing 7 M urea. The Biotin-labeled-RNA was transferred to nylon membranes and crosslinked using an ultraviolet crosslinker and was detected using a Chemiluminescent Biotin-labeled Nucleic Acid Detection Kit (Beyotime, D3308).

RNA transporting assay

The GDF9 cRNA was transcribed using a HiScribe T7 High Yield RNA Synthesis Kit (E2060). The RNA (500 ng/µl) was injected into the nucleus of WT and KO oocytes. The oocytes were fixed by 2% PFA at 0 min, 30 min and 60 min. Then ISH was performed according to standard protocol (Jansova et al., 2021). Briefly, the Cy5-labeled oligo(dT) or specific DNA probes were generated. Oocytes were fixed with 2% PFA (Sangon Biotech) for 30 min at room temperature and permeabilized in 2% Triton X-100 in PBS for 10 min with RNase Inhibitor. Then oocytes were incubated with 100 µl hybridization buffer containing 100 nM hybridization probes overnight at 37°C. After hybridization, oocytes were washed three times by 2×SSC to remove extra probes.

Detection of RNA synthesis and protein synthesis in oocytes

GV oocytes were treated with 2 mM EU (Thermo Fisher Scientific) at 37°C with 5% CO_2 for 1 h and then fixed in 2% PFA for 1 h and permeabilized in

0.5% Triton X-100 in PBS for 20 min. Oocytes were stained using a Click-iT RNA Alexa Fluor 594 kit (Thermo Fisher Scientific) to detect nascent RNA. DNA was labeled using Hoechst 33342 for 10 min. To detect protein synthesis, oocytes were cultured in methionine-free medium (Gibco) supplemented with 1% dialyzed fetal bovine serum (10,000 MW; Sigma-Aldrich) and 50 µM HPG for 1 h. HPG was detected using a Click-iT HPG Alexa Fluor Protein Synthesis Assay Kit (Life Technologies) according to the manufacturer's instructions. All images were captured on an LSM 880 laser scanning confocal microscope (Zeiss).

Library construction and RNA-seq analysis

GV and MII oocytes were collected from WT and *Patl2*$^{-/-}$ female mice (7- to 8-weeks-old). Total RNA from oocytes was extracted using a RNeasy Mini Kit (Qiagen). The mRNA-GFP and mCherry were sparked into the lysed sample for RNA isolation according to a previously reported method (Yu et al., 2016). Then sequencing libraries were prepared according to the cDNA Synthesis, Amplification and Library Generation Kit (E6420, New England Biolabs). Library samples were sequenced on the Illumina Novaseq 6000 instrument by Genergy Biotechnology Co. The raw data were handled by Skewer, and data quality was checked by FastQC v0.11.2. The read length was 2×150 bp. Clean reads were aligned to the *Mus musculus* UCSCmm9 references using STAR and StringTie. The expression levels of the genes were quantified using fragments per kilobase of transcript per million mapped fragments (FPKM). The total mRNA copy was calculated as its FPKM normalized to the FPKM of exogenous *GFP*/*mCherry*. The FPKMs of the RNA-seq results are listed in Tables S3, S5 and S6.

Statistical analysis

Quantitation of western blotting results was performed with ImageJ software, and statistical analyses were performed using GraphPad Prism. *P*-values were calculated with two-tailed unpaired Student's *t*-test or chi-square test as described in the figure and table legends. **P*<0.05; ***P*<0.01 and ****P*<0.001 (*P*>0.05, not significant).

Acknowledgements

We thank Yinghua Jiang for providing help with confocal imaging, and the Public Technology Platform of Shanghai Medical College.

Competing interests

The authors declare no competing or financial interests.

Author contributions

Conceptualization: Q.S., L.W.; Methodology: R.Q., R.Y., J.M., X.G.; Software: B.C.; Investigation: Z. Zhang, R.L., H.Z., W.W., Y.Z.; Data curation: Z. Zhang, R.L., Q.L., R.Q., Z. Zhou, J.M., X.G.; Writing - original draft: Z. Zhang; Writing - review & editing: Z. Zhang; Supervision: Q.S., L.W.; Project administration: Q.S., L.W.; Funding acquisition: Z. Zhang, Q.S., L.W.

Funding

This work was supported by the National Key Research and Development Program of China (2021YFC2700100), the Basic Science Center Program of the National Natural Science Foundation of China (82288102), the National Natural Science Foundation of China (32130029, 82171643, 81971450, 82001538, 81971382), the Guangdong Science and Technology Department–Hong Kong-Macao Joint Innovation Project (2020A0505140003) and the National Key Research and Development Program for Young Scientists (2022YFC2702300).

Data availability

RNA-seq raw data have been deposited in the Genome Sequence Archive in National Genomics Data Center, China National Center for Bioinformation/Beijing Institute of Genomics, Chinese Academy of Sciences under accession number CRA009231.

Peer review history

The peer review history is available online at https://journals.biologists.com/dev/lookup/doi/10.1242/dev.201572.reviewer-comments.pdf.

References

Chen, B., Zhang, Z., Sun, X., Kuang, Y., Mao, X., Wang, X., Yan, Z., Li, B., Xu, Y., Yu, M. et al. (2017). Biallelic mutations in PATL2 cause female infertility characterized by oocyte maturation arrest. *Am. J. Hum. Genet.* **101**, 609-615. doi:10.1016/j.ajhg.2017.08.018

Christou-Kent, M., Kherraf, Z. E., Amiri-Yekta, A., Le Blévec, E., Karaouzène, T., Conne, B., Escoffier, J., Assou, S., Guttin, A., Lambert, E. et al. (2018). PATL2 is a key actor of oocyte maturation whose invalidation causes infertility in women and mice. *EMBO Mol. Med.* **10**, e8515. doi:10.15252/emmm.201708515

Clerici, M., Faini, M., Muckenfuss, L. M., Aebersold, R. and Jinek, M. (2018). Structural basis of AAUAAA polyadenylation signal recognition by the human CPSF complex. *Nat. Struct. Mol. Biol.* **25**, 135-138. doi:10.1038/s41594-017-0020-6

Coticchio, G., Dal Canto, M., Mignini Renzini, M., Guglielmo, M. C., Brambillasca, F., Turchi, D., Novara, P. V. and Fadini, R. (2015). Oocyte maturation: gamete-somatic cells interactions, meiotic resumption, cytoskeletal dynamics and cytoplasmic reorganization. *Hum. Reprod. Update* **21**, 427-454. doi:10.1093/humupd/dmv011

Cox, J. and Mann, M. (2008). MaxQuant enables high peptide identification rates, individualized p.p.b.-range mass accuracies and proteome-wide protein quantification. *Nat. Biotechnol.* **26**, 1367-1372. doi:10.1038/nbt.1511

Ding, Z.-M., Huang, C.-J., Jiao, X.-F., Wu, D. and Huo, L.-J. (2017). The role of TACC3 in mitotic spindle organization. *Cytoskeleton* **74**369-378. doi:10.1002/cm.21388

Eichhorn, S. W., Subtelny, A. O., Kronja, I., Kwasnieski, J. C., Orr-Weaver, T. L. and Bartel, D. P. (2016). mRNA poly(A)-tail changes specified by deadenylation broadly reshape translation in Drosophila oocytes and early embryos. *eLife* **5**, e16955. doi:10.7554/eLife.16955

Groisman, I., Huang, Y. S., Mendez, R., Cao, Q. and Richter, J. D. (2001). Translational control of embryonic cell division by CPEB and maskin. *Cold Spring Harb. Symp. Quant. Biol.* **66**, 345-351. doi:10.1101/sqb.2001.66.345

Huang, L., Tong, X., Wang, F., Luo, L., Jin, R., Fu, Y., Zhou, G., Li, D., Song, G., Liu, Y. et al. (2018). Novel mutations in PATL2 cause female infertility with oocyte germinal vesicle arrest. *Hum. Reprod.* **33**, 1183-1190. doi:10.1093/humrep/dey100

Huang, L., Wang, Y., Lu, F., Jin, Q., Song, G., Ji, J., Luo, L., Jin, R. and Tong, X. (2022). Novel mutations in NLRP5 and PATL2 cause female infertility characterized by primarily oocyte maturation abnormality and consequent early embryonic arrest. *J. Assist. Reprod. Genet.* **39**, 711-718. doi:10.1007/s10815-022-02412-4

Jansova, D., Aleshkina, D., Jindrova, A., Iyyappan, R., An, Q., Fan, G. and Susor, A. (2021). Single molecule RNA localization and translation in the mammalian oocyte and embryo. *J. Mol. Biol.* **433**, 167166. doi:10.1016/j.jmb.2021.167166

Kang, M. K. and Han, S. J. (2011). Post-transcriptional and post-translational regulation during mouse oocyte maturation. *BMB Rep.* **44**, 147-157. doi:10.5483/BMBRep.2011.44.3.147

Liu, Y., Nie, H., Liu, H. and Lu, F. (2019). Poly(A) inclusive RNA isoform sequencing (PAIso-seq) reveals wide-spread non-adenosine residues within RNA poly(A) tails. *Nat. Commun.* **10**, 5292. doi:10.1038/s41467-019-13228-9

Liu, Z., Zhu, L., Wang, J., Luo, G., Xi, Q., Zhou, X., Li, Z., Yang, X., Duan, J., Jin, L. et al. (2020). Novel homozygous mutations in PATL2 lead to female infertility with oocyte maturation arrest. *J. Assist. Reprod. Genet.* **37**, 841-847. doi:10.1007/s10815-020-01698-6

Liu, Y., Zhang, Y., Wang, J. and Lu, F. (2022). Transcriptome-wide measurement of poly(A) tail length and composition at subnanogram total RNA sensitivity by PAIso-seq. *Nat. Protoc.* **17**, 1980-2007. doi:10.1038/s41596-022-00704-8

Ma, J., Flemr, M., Strnad, H., Svoboda, P. and Schultz, R. M. (2013). Maternally recruited DCP1A and DCP2 contribute to messenger RNA degradation during oocyte maturation and genome activation in mouse. *Biol. Reprod.* **88**, 11. doi:10.1095/biolreprod.112.105312

Maddirevula, S., Coskun, S., Alhassan, S., Elnour, A., Alsaif, H. S., Ibrahim, N., Abdulwahab, F., Arold, S. T. and Alkuraya, F. S. (2017). Female infertility caused by mutations in the oocyte-specific translational repressor PATL2. *Am. J. Hum. Genet.* **101**, 603-608. doi:10.1016/j.ajhg.2017.08.009

Marnef, A. and Standart, N. (2010). Pat1 proteins: a life in translation, translation repression and mRNA decay. *Biochem. Soc. Trans.* **38**, 1602-1607. doi:10.1042/BST0381602

Marnef, A., Maldonado, M., Bugaut, A., Balasubramanian, S., Kress, M., Weil, D. and Standart, N. (2010). Distinct functions of maternal and somatic Pat1 protein paralogs. *RNA* **16**, 2094-2107. doi:10.1261/rna.2295410

Mendez, R., Barnard, D. and Richter, J. D. (2002). Differential mRNA translation and meiotic progression require Cdc2-mediated CPEB destruction. *EMBO J.* **21**, 1833-1844. doi:10.1093/emboj/21.7.1833

Minshall, N., Reiter, M. H., Weil, D. and Standart, N. (2007). CPEB interacts with an ovary-specific eIF4E and 4E-T in early Xenopus oocytes. *J. Biol. Chem.* **282**, 37389-37401. doi:10.1074/jbc.M704629200

Nakamura, Y., Tanaka, K. J., Miyauchi, M., Huang, L., Tsujimoto, M. and Matsumoto, K. (2010). Translational repression by the oocyte-specific protein P100 in Xenopus. *Dev. Biol.* **344**, 272-283. doi:10.1016/j.ydbio.2010.05.006

Ozgur, S., Chekulaeva, M. and Stoecklin, G. (2010). Human Pat1b connects deadenylation with mRNA decapping and controls the assembly of processing bodies. *Mol. Cell. Biol.* **30**, 4308-4323. doi:10.1128/MCB.00429-10

Passmore, L. A. and Coller, J. (2022). Roles of mRNA poly(A) tails in regulation of eukaryotic gene expression. *Nat. Rev. Mol. Cell Biol.* **23**, 93-106. doi:10.1038/s41580-021-00417-y

Pfaffl, M. W. (2001). A new mathematical model for relative quantification in real-time RT-PCR. *Nucleic Acids Res.* **29**, e45. doi:10.1093/nar/29.9.e45

Picton, H., Briggs, D. and Gosden, R. (1998). The molecular basis of oocyte growth and development. *Mol. Cell. Endocrinol.* **145**, 27-37. doi:10.1016/S0303-7207(98)00166-X

Racki, W. J. and Richter, J. D. (2006). CPEB controls oocyte growth and follicle development in the mouse. *Development* **133**, 4527-4537. doi:10.1242/dev.02651

Rother, R. P., Frank, M. B. and Thomas, P. S. (1992). Purification, primary structure, bacterial expression and subcellular distribution of an oocyte-specific protein in Xenopus. *Eur. J. Biochem.* **206**, 673-683. doi:10.1111/j.1432-1033.1992.tb16973.x

Sang, Q., Zhang, Z., Shi, J., Sun, X., Li, B., Yan, Z., Xue, S., Ai, A., Lyu, Q., Li, W. et al. (2019). A pannexin 1 channelopathy causes human oocyte death. *Sci. Transl. Med.* **11**, eaav8731. doi:10.1126/scitranslmed.aav8731

Setoyama, D., Yamashita, M. and Sagata, N. (2007). Mechanism of degradation of CPEB during Xenopus oocyte maturation. *Proc. Natl. Acad. Sci. USA* **104**, 18001-18006. doi:10.1073/pnas.0706952104

Sha, Q. Q., Dai, X. X., Dang, Y., Tang, F., Liu, J., Zhang, Y. L. and Fan, H. Y. (2017). A MAPK cascade couples maternal mRNA translation and degradation to meiotic cell cycle progression in mouse oocytes. *Development* **144**, 452-463. doi:10.1242/dev.144410

Sha, Q. Q., Zheng, W., Wu, Y. W., Li, S., Guo, L., Zhang, S., Lin, G., Ou, X. H. and Fan, H. Y. (2020). Dynamics and clinical relevance of maternal mRNA clearance during the oocyte-to-embryo transition in humans. *Nat. Commun.* **11**, 4917. doi:10.1038/s41467-020-18680-6

So, C., Seres, K. B., Steyer, A. M., Monnich, E., Clift, D., Pejkovska, A., Mobius, W. and Schuh, M. (2019). A liquid-like spindle domain promotes acentrosomal spindle assembly in mammalian oocytes. *Science* **364**, eaat9557. doi:10.1126/science.aat9557

Stebbins-Boaz, B., Hake, L. E. and Richter, J. D. (1996). CPEB controls the cytoplasmic polyadenylation of cyclin, Cdk2 and c-mos mRNAs and is necessary for oocyte maturation in Xenopus. *EMBO J.* **15**, 2582-2592. doi:10.1002/j.1460-2075.1996.tb00616.x

Stebbins-Boaz, B., Cao, Q., De Moor, C. H., Mendez, R. and Richter, J. D. (1999). Maskin is a CPEB-associated factor that transiently interacts with eIF-4E. *Mol. Cell* **4**, 1017-1027. doi:10.1016/S1097-2765(00)80230-0

Susor, A., Jansova, D., Cerna, R., Danylevska, A., Anger, M., Toralova, T., Malik, R., Supolikova, J., Cook, M. S., Oh, J. S. et al. (2015). Temporal and spatial regulation of translation in the mammalian oocyte via the mTOR-eIF4F pathway. *Nat. Commun.* **6**, 6078. doi:10.1038/ncomms7078

Swetloff, A., Conne, B., Huarte, J., Pitetti, J. L., Nef, S. and Vassalli, J.-D. (2009). Dcp1-bodies in mouse oocytes. *Mol. Biol. Cell* **20**, 4951-4961. doi:10.1091/mbc.e09-02-0123

Wang, M., Guo, Y., Wang, M., Zhou, T., Xue, Y., Du, G., Wei, X., Wang, J., Qi, L., Zhang, H. et al. (2017). The glial cell-derived neurotrophic factor (GDNF)-responsive phosphoprotein landscape identifies raptor phosphorylation required for spermatogonial progenitor cell proliferation. *Mol. Cell. Proteomics* **16**, 982-997. doi:10.1074/mcp.M116.065797

Yu, C., Ji, S.-Y., Sha, Q.-Q., Dang, Y., Zhou, J.-J., Zhang, Y.-L., Liu, Y., Wang, Z.-W., Hu, B., Sun, Q.-Y. et al. (2016). BTG4 is a meiotic cell cycle-coupled maternal-zygotic-transition licensing factor in oocytes. *Nat. Struct. Mol. Biol.* **23**, 387-394. doi:10.1038/nsmb.3204

Wu, L., Chen, H., Li, D., Song, D., Chen, B., Yan, Z., Lyu, Q., Wang, L., Kuang, Y., Li, B. et al. (2019). Novel mutations in PATL2: expanding the mutational spectrum and corresponding phenotypic variability associated with female infertility. *J. Hum. Genet.* **64**, 379-385. doi:10.1038/s10038-019-0568-6

Wu, T., Dong, J., Fu, J., Kuang, Y., Chen, B., Gu, H., Luo, Y., Gu, R., Zhang, M., Li, W. et al. (2022). The mechanism of acentrosomal spindle assembly in human oocytes. *Science* **378**, eabq7361. doi:10.1126/science.abq7361